Locating groundwater resources for Aboriginal communities in remote and arid parts of South Australia

D. Pedler-Jones

Supervisor: Graham Heinson

Locating groundwater resources for Aboriginal communities in remote and arid parts of South Australia

David Pedler-Jones 1148574

Abstract

Aboriginal communities in remote areas of South Australia require access to bore water for their non-potable supplies due to the aridity of the region. This water is often found in deep, fractured rock aquifers. Due to the anisotropic and heterogeneous nature of fractured rock aquifers, there is a significant risk of drilling costly dry bore holes in the attempt to find water. This project is a pilot study to gauge the effectiveness of magnetotellurics - a geophysical method that images the distribution of electrical conductivity in the subsurface - in mapping and characterising fractured rock aquifers in order to reduce the risk of drilling dry bore holes. This survey was carried out in the Nipapanha Community, in the Northern Flinders Ranges, South Australia. There is a need for an increase in bore water supply from the local fractured rock aquifer. Geophysical, hydrogeological and structural research has been carried out in the area, which will act as a guide for this survey, so that knowledge and techniques learned may be applied in poorly constrained areas.

Magnetotelluric data were recorded at 3000Hz and 500Hz over 40 sites around the target area in order to create a series of 5 2D profiles as well as a map of phase tensors at various frequencies. Controlled source magnetotelluric data from a previous survey carried out by Zonge Engineering were obtained and reprocessed and inverted to create a series of 6 inversions in order to increase coverage of the survey. Interpretation of the inversions and phase tensors in conjunction with hydrogeological information was able to identify areas of anomalous apparent conductivity, possibly corresponding to increased water content. Predominant directions of conductivity, corresponding to fracture orientation throughout the area were also identified.

Introduction

Many Aboriginal communities in remote and arid parts of South Australia currently rely on groundwater resources located in deep aquifers (>50m to the water table) in fractured rock for non-potable water supplies. Rainfall in these areas is highly variable, ranging from periods of drought to occasional very high rainfall events. The quality and quantity of water available from fractured frock aquifers is variable on a small scale, with unsuccessful bores drilled within metres of productive bores.

Due to the remoteness of these communities, drilling dry boreholes can be a very costly exercise and it is hoped that the use of magnetotellurics (MT) will be able to reduce this risk. This was achieved by using magnetotelluric data in a grid over prospective aquifers to image two dimensional slices and phase tensor profiles through the geology to better understand the dimensionality of electrical conductivity in the sub-surface. By then applying Archie's Law, which describes the relationship between conductivity, pore space and water salinity, we can better define the flow and distribution of water in the subsurface.

Fractures within the aquifers can be difficult to detect for a combination of reasons:

- Bulk porosities of fractured rock aquifers are generally low, typically less than 1%, and will reduce with depth; therefore the bulk electrical conductivity will be only marginally dependent on water saturation.
- Fractures display spatial heterogeneity, in terms of their length, orientation, aperture and connection, therefore the electrical conductivity will depend on the position and orientation of measurement
- The analogy between the flux of fluid and electrical currents is only partially correct, in practice electric currents have high mobility and can flow in all directions under various electric potential gradients, whereas fluid flow is generally downwards under gravitational pressure potential.

This project is based in the Aboriginal community of Nipapanha, located 500km north of Adelaide between Lake Frome and Lake Torrens in the Arrowie Basin of the Northern Flinders Ranges. The community was established in the 1930's in an area with only a spring fed creek as a water supply (Costar *et al.* 2008). Bore water is currently supplied by a dual reticulation system sourcing water from two wells with salinity in the ~1000mg/L TDS region and yields of 2.2 and 12 L/s which have been declining (Costar *et al.* 2009).

This project is a pilot study in a 2 year program, as there are a number of geological and geophysical constraints already placed upon the area around the Nipapanha community, with knowledge gained from this project used to interpret data from the Anangu Pitjantjatjara Yankunytjatjara lands next year.

Previous Studies

The geophysical methods of direct current (DC) and in particular, electromagnetics (EM) are useful for providing a three dimensional framework to work from when describing fluid flow through heterogeneous fractured mediums. They are more effective than other methods such as borehole logging, drill core investigation, packer tests and pump tests due to these methods failing to quantify bulk properties of the whole medium; EM methods produce volumetric data which can produce bulk hydraulic parameters as opposed to point source test results (Skinner & Heinson 2004).The use of magnetotellurics to image aquifer systems has been carried out in multiple areas world-wide (Turberg *et al.* 1994, Newman *et al.* 2008, Arango *et al.* 2009, Chandrasekhar *et al.* 2009).

The Llucmajor aquifer system in Spain was mapped with a high degree of success by using 3D forward modelling taking into account the impedance tensor. This approach allowed delineation of aquifer features with resistivities ranging across 2 orders of magnitude and depths of up to 600 metres. By integrating exploration borehole logs and 2D impedance profiles, the workers were able to create an accurate 3D model that images layers of the aquifer system that vary in thickness, saturation and connectivity in three dimensions (Arango *et al.* 2009).While most of these papers are concerned with the magnetotelluric characterization of porous aquifers, some work has been done on fractured rock aquifers, e.g. (Moeck *et al.* 2007)

The groundwater flux of the fractured rock aquifer system of the Central Algarve Basin in Portugal was mapped with the use of stress tensor orientations coupled with magnetotelluric, electromagnetic and hydrogeological data. By integrating these data sets the workers were able to reveal significant relationships between hydraulically conductive structures and fault and fracture

kinematics within the current stress field. They concluded that magnetotellurics combined with tectonic analysis, remote sensing and hydrogeological investigation is a useful tool in the investigation of groundwater flow in fractured rock systems (Moeck *et al.* 2007).

The differences in the way porous aquifers and fractured aquifers conduct groundwater make it a much less certain process when using magnetotellurics to image fractured rock aquifers. Characterising the flow of any fluid through fractured rock represents a unique challenge due to extreme contrasts in hydraulic conductivity between fractures and the surrounding matrix, ranging from well connected fracture networks providing a very permeable system for fluid flow down to totally sealed fractures disallowing fluid flow. In order to characterise a network of fractured rock aquifers it is necessary to determine the percentage of fractures in each network that is conductive, the degree of conductivity, and what effect this has on the overall anisotropy of the rock mass (Faybishenko 2000).

When considering the differences between fractured rock and porous rock aquifers, it is important to realise that there is a spectrum of different combinations of fractured and porous aquifer systems. Porous systems can range from homogenous to heterogeneous, where variations in grain size cause preferential flow paths within the matrix. There can also be fractured porous media with good permeability throughout the matrix leading to good connectivity, and fractured porous media that is not very permeable leading to poor fracture-matrix connectivity. There are also purely fractured systems with negligible porosity (Cook 2003). Structural, hydrogeological and geophysical studies have previously been carried out in the Nepabunna area, making it ideal for a proof of concept test area, as there are multiple studies to compare results against.

A hydrogeological investigation carried out by Read (1981) identified the various hydrogeological properties of the lithologies present in the Nepabunna area. Production from wells to the north and west of Nepabunna was strongly dependent on seasonal recharge into the Mt McKinlay creek. It was suggested that structure was a more important control on permeability than lithology, but another study by Read (1984) suggested that diminishing returns from a well field in the Nepabunna Siltstone due to dewatering was due to poor hydrogeological properties of the siltstone. The Wilkawillina Limestone was then identified as a potential regional aquifer due to its hydrogeological properties and good performance in pumping tests.

Previous geophysical work has been carried out in the Nipapanha community by the Department of Water, Land and Biodiversity Conservation. Their study was based around using controlled source audio-magnetotellurics (CSAMT) to create a series of east-west aligned profiles where they believed the prospective area to be, due to a juxtaposition of the main aquifer unit and a creek with a reasonable sized catchment area. Their study was not very effective due to the use of CSAMT only providing scalar data and therefore 1D inversion profiles. This level of information was insufficient to properly characterise the distribution of water throughout the aquifer due to there being an insufficient contrast of water filled fractures against the matrix (most likely because the fracture system was not sufficiently prevalent, large or saturated) and a drilling program was not recommended with this data as a guide (Costar *et al.* 2008). This project aims to expand upon the work by Costar et al. (2008) by using AMT to create a series of 2D inversions and phase tensor maps to provide greater information about the direction of electrical conductivity and therefore water

flow and fracture orientation, rather than the exact distribution; it is hoped that this information will provide a better groundwork for a drilling program to be based on.

Geology

Regional Geological Framework:

The Northern Flinders Ranges display broad, open dome and basin-shaped folds possibly formed by an early phase of meridonal folding and a concurrent phase of east-north east trending fold pattern. It has been suggested by Dyson (1998, 1999) the dome and basin formations are caused by Late Precambrian to Early Cambrian salt tectonics with the Delamerian Orogeny causing minor tightening of folds (Costar *et al.* 2009). The regional east-northeast and local west-northwest trend of the fold axes provide evidence for roughly north-south oriented shortening (Paul *et al.* 1999).

According to Dyson (2005), the open dome structures are centred on apparent diapiric intrusions. Synclines are rimmed by diapirs that were formed due to salt withdrawal and into which sediments of the Hawker and Wilpena Groups were deposited. The synclines were subject to only minor late stage compression and so remain fairly open structures, with their structural orientation dominantly northwest and northeast which is thought to coincide with the main structural lineaments that are associated with late Neoproterozoic rifting.

Structure:

The Nipapanha Community is located within the Nepabunna Synclinorium, a structure composed of two east-west trending synclines separated by an anticline. The synclines tighten towards the west causing possible minor attenuation of the bedding thickness, but open out towards the east (Costar *et al.* 2009). A number of small faults have been identified, although they appear to be relatively old as some have been filled in with calcite and a few others remain open. At the outcrop level the most obvious feature is the primary east-west trending cleavage which has developed parallel with the axial plane of folding (Read 1981).

Stratigraphy:

The stratigraphy of the Nepabunna Synclinorium ranges in age from Late Precambrian (Wilpena Group) to Early Cambrian (Hawker Group) in age. Previous investigations have identified the Wilkawillina Limestone of the Hawker Group as a potential regional aquifer target. The Wilkawillina Limestone is classified as typically biohermal and stromatolitic, regularly dolomitic and oolitic, interbedded with grey calcareous siltstone, limonitic siltstone and minor thin bedded sandstone. This formation defines the outcrop of the plunging synclines of the Nepabunna Synclinorium along with the Nepabunna Siltstone, which is classified as a dark blue-grey to greyish green calcareous siltstone with minor thin beds of limestone (Costar *et al.* 2009).

The Wilkawillina limestone has been identified as the main unit of interest for hydrogeological purposes, and can be further split into upper and lower units. The lower unit is classified as a clean massive limestone, which may have moderate yield in places, especially where they are crossed by a creek for recharge. The upper unit is classified as interbedded limestone and siltstone, and has only given poor yields where it has been drilled in the past (Costar *et al.* 2008).

Method

Magnetotelluric method:

Magnetotellurics is a field of geophysics used to provide information about the distribution of electrical conductivity throughout the Earth's crust and mantle. It is flexible in that in can sense from a few metres to hundreds of kilometres depth. It involves measuring the naturally occurring electromagnetic field present between the ionosphere and ground to measure the distribution of electric resistivity throughout the earth. It relies on simultaneously measuring the fluctuations of electrical and magnetic components in different dimensions in order to determine the distribution, strike and skew of electrical resistivity (Smirnov *et al.* 2008, Arango *et al.* 2009). When measuring the local magnetic **H** and electrical fields **E** during a magnetotelluric survey, even though there can be localised distortion of the magnetic field, we can assume that the measured local field **H** is a good approximation of the regional field $\mathbf{H_R}$.If the measured electrical field is distorted by heterogeneities in the sub-surface, we can say that this measured field, **E**, has been distorted from the regional electrical field, $\mathbf{E_R}$, by the distortion tensor, **D**, i.e. $\mathbf{E = D\ E_R}$. **D** acts by distorting the magnitude and direction of the measured electrical field.

The impedance **Z** is the relationship that links the measured electrical field and magnetic field, i.e. $\mathbf{E = Z\ H}$. If there is no distortion, the regional impedance $\mathbf{Z_R}$ can be given by $\mathbf{E_R = Z_R\ H_R}$. The relationship between the observed and regional impedance is therefore $\mathbf{Z = D\ Z_R}$ (Caldwell *et al.* 2004, Bibby *et al.* 2005).

The skin depth equation is given by:

$$\delta = \sqrt{2/\sigma\mu\omega}$$

Where σ is the conductivity, μ is the magnetic permeability, ω is the frequency and δ is the depth. Due to the fact that magnetic permeability, μ, does not vary substantially in the earth, this equation can be re-written as $\delta(T) \approx 500\sqrt{T\varrho}$ where T is the period in seconds and ϱ is the apparent resistivity in ohm.m.

This equation is very powerful, as it gives the relationship between the depth that the equipment is sensitive to and the frequency that it corresponds to. This can be interpreted as saying that for a given resistivity of the earth, studying longer period wavelengths will correspond to deeper depths, and for a given period the depth of investigation will increase for an increase in resistivity (Smirnov *et al.* 2008).

The bandwidth of frequencies used in magnetotelluric studies ranges from 10^4 Hz to 10^{-4} Hz, which corresponds to depths of around 50m-500km for the average earth conductivity. The range of frequencies are derived from a few different sources, the most important signal covering 10^4 Hz to 10 Hz coming from meteorological activity (lightning strikes). A lightning strike causes a radially expanding magnetic field which propagates through the atmosphere with almost no attenuation, and at a distance far enough from the strike will appear as a uniform plane-wave source. Due to the global frequency of thunderstorms, especially around the equator, this is a reliable and useful source. Around the bandwidth of 10^1 Hz to 10^{-1} Hz there is almost no natural source of energy to provide a magnetotelluric signal; this can be a problem as the skin depth of these frequencies

roughly corresponds to 1.5km to 15km, which is the depth of interest for many studies. The signal in the bandwidth of 10^{-1} Hz to 10^{-4} Hz is provided by magnetic pulsations and magnetic storms. The pulsations are caused by electrons resonating in the ionosphere; these resonances occur over a wide area and behave like a plane-wave source. Magnetic storms are caused by solar activity disrupting the geomagnetic field which acts as a uniform inducing field at most latitudes of the earth (Simpson & Bahr 2005).

The phase tensor is a method of using the observed data to plot a series of ellipses which provide information about the strike and complexity (or degree of 3-dimensionality) of the electrical resistivity structure. These ellipses are therefore a powerful tool to visually analyse the degree of anisotropy of fracture alignment if we use the logic that fractures which carry water will have a higher electrical conductivity than the surrounding rock (Skinner & Heinson 2004, Rayner *et al.* 2007). Therefore if the majority of fractures are aligned in the same direction, there will be a greater electrical conductivity overall in that direction, than orthogonal to it, which will be revealed by the phase tensor ellipses (Caldwell *et al.* 2004, Bibby *et al.* 2005). The phase tensor can be derived by splitting the regional and local impedance tensors **Z** and $\mathbf{Z_R}$ into real (**X**) and imaginary (**Y**) parts.

$\mathbf{Z} = \mathbf{X} + i\,\mathbf{Y}$ and $\mathbf{Z_R} = \mathbf{X_R} + i\,\mathbf{Y_R}$

$\mathbf{Z = D\,Z_R}$ can be rewritten as 2 equations, $\mathbf{X = D\,X_R}$ and $\mathbf{Y = D\,Y_R}$

The components of **Z** can be defined as $Z = \begin{bmatrix} Z_{xx} & Z_{xy} \\ Z_{yx} & Z_{yy} \end{bmatrix}$.

These components contain information about the dimensionality of the subsurface, and can be used to determine if it is 1D, 2D or 3D.

The phase tensor is defined as $\mathbf{\Phi = X^{-1}\,Y}$ where $\mathbf{X^{-1}}$ is the inverse of **X** (the real part of the impedance tensor **Z**). The phase tensor can also be defined in terms of the regional field by

$\mathbf{\Phi = X^{-1}\,Y = (D\,X_R)^{-1}(D\,Y_R) = X_R^{-1}D^{-1}D\,Y_R = X_R^{-1}\,Y_R = \Phi_R}$

Thereby, as expected, the phase will behave independent of the distortion tensor **D** which affects the impedance tensor (Caldwell *et al.* 2004, Bibby *et al.* 2005).

The phase tensor is a real, second rank tensor, which means that it is defined by three independent scalar values ($\mathbf{\Phi}$max, $\mathbf{\Phi}$min and $\boldsymbol{\beta}$) and a direction ($\boldsymbol{\alpha}$).

$\boldsymbol{\beta}$ is a measure of the asymmetry of the phase tensor, higher values correspond to greater asymmetry.

$$\boldsymbol{\beta} = \frac{1}{2}\boldsymbol{tan}^{-1}\left(\frac{\mathbf{\Phi_{12} - \Phi_{21}}}{\mathbf{\Phi_{11} + \Phi_{22}}}\right).$$

$\boldsymbol{\alpha}$ is the direction of the phase tensor, and expresses the tensor's dependence on the co-ordinate system.

$$\boldsymbol{\alpha} = \frac{1}{2}\boldsymbol{tan}^{-1}\left(\frac{\mathbf{\Phi_{12} + \Phi_{21}}}{\mathbf{\Phi_{11} - \Phi_{22}}}\right).$$

The phase tensor is fully defined by

$$\Phi = R^T(\alpha - \beta)\begin{bmatrix}\Phi\max & 0\\ 0 & \Phi\min\end{bmatrix}R(\alpha + \beta).$$

where R(α+β) is the rotation matrix, and R^T is the inverse rotation matrix.

$$R(\alpha + \beta) = \begin{bmatrix} cos(\alpha + \beta) & sin(\alpha + \beta)\\ -sin(\alpha + \beta) & cos(\alpha + \beta)\end{bmatrix}.$$

The phase tensor will behave differently for 1D, 2D and 3D cases.

For a 1D case the graphical representation of the ellipse will be a circle due to equal values for **Φ**max and **Φ**min. An example of a 1D scenario would be a uniform stack of layers, such as an homogeneous and isotropic sedimentary aquifer.

For 2D cases **Φ**max and **Φ**min will have different values and therefore the phase tensor will form an ellipse and represent the strike of electrical conductivity. However, the third co-ordinate invariant **β** will be zero and the phase tensor will be symmetric. An example of a 2D scenario would be where the earth varies in 2 dimensions, but remains constant in the third, such as a fault.

For 3D cases **Φ**max and **Φ**min will have different values, once again causing the phase tensor to appear as an ellipse with the major axis showing the strike of electrical conduction and **β** will be non zero which measures the degree of asymmetry of the tensor. An example of a 3D structure would be an ore body varying in all 3D dimensions. (Caldwell *et al.* 2004).

Magnetotellurics can be used to create a 3D image of the subsurface by deploying the stations in a grid over the study area and then inverting and forward modelling the data to create a 3D image of electrical resistivity (Garcia *et al.* 1999).

Field Deployment:

Field work was carried out in June of 2010, taking roughly a week to complete. 14 instruments in total were used, utilising Tinker & Rasor copper-copper sulphate half cell reference electrodes to measure the electric fields, and broadband induction magnetometers to measure the magnetic fields.

Each station comprised a set of 3 electrodes oriented in the N-S and E-W directions at 90° to each other, with dipole lengths as close to 50m as practically allowable, a set of 2 induction coil magnetometers also aligned N-S and E-W. These were plugged into a logger which records the time-series data to a hard drive, a GPS receiver to ensure accurate measurements of time and location and a car battery to provide power. Once set up, a laptop was used to connect to the logger to check the signal and set the sampling rate. For the purposes of this experiment the loggers were first set to record at 3000 Hz for at least 30 minutes in order to record long enough obtain enough signal to achieve an acceptable signal to noise ratio, then set to 500 Hz overnight. This strategy was used to obtain good signal to noise ratio in both the long and short period wavelengths present in the area due to the rocky and undulating terrain causing distortion of the signal. Two sites were set up initially near the survey area in areas thought to have a good signal to noise ratio to run for the whole duration of the survey and act as remote references for the processing stage.

A preliminary aerial photo investigation for site selection taking into account distance from established tracks and power lines as well as difficulty of terrain yielded a possible 60 sites, once in the field it was realised that the terrain was more difficult than realised and sites were selected based on ease of access while maintaining a 200-300m separation. In all, 40 sites and 2 remote reference sites were collected.

Data Processing:

Data were recorded and inspected as a time series of field values which were then subjected to a Fourier transformation, which seeks to represent the time domain data in the frequency domain. This was done using the BIRRP code. The Fourier transformed files were then converted to a set of files for use with the modelling software, WinGLink, according to various parameters, such as remote referencing and coherence thresholds.

Remote referencing works by assuming that the magnetic field over the entire region should change constantly. It compares the magnetic fields from the site and the remote reference and any signal that is not common is interpreted as noise and ignored. Coherence thresholds seek to improve the signal to noise ratio of the data by rejecting parts of the signal that have a coherence value that is lower than whatever specific value the threshold was set at. If a site was particularly noisy, the threshold could be set as high as 0.7, and only a small portion of the data would be used. This process gives a smoother model with a better RMS value (a measure of how well the observed data fits the model) (Chave & Thomson 2003). The apparent resistivity and phase vs. frequency plots were then investigated manually in WinGLink, with any clearly noisy frequencies being masked out. These frequencies were commonly 50Hz, and most frequencies above 100Hz, and below 1Hz.

Results

The figures for the result section (figures 2,3,4,5,6,7,8,9,10,11 and 12) were chosen to best provide information about the area by using roughly perpendicular profiles that cover all the sites, as well as the structures and areas of importance. They show 2D inversions of profiles NS1, NS2, EW1, EW2 and EW3, as well as inversions of Zonge profiles 4600, 4900, 5180, 5450, 5650 and 5850. Phase tensor profiles of 94Hz, 70hz and 23Hz, as well as a pseudo section of profile NS1.

Profiles NS1 and NS2 shows increasing resistivity with depth and a synclinal feature. Profiles EW1, EW2 and EW3 show increasing resistivity with depth, a structural plunge towards the east and zones of higher apparent conductivity separated by a resistive band. The Zonge profiles show continuation of anomalous conductive units across the profile relating to a productive bore. The phase tensor profiles show dominant regional conductivity in the northeast-southwest direction, with shallower features ranging from northeast-southwest to northwest-southeast conductance.

Discussion

When attempting to interpret the 2D inversions produced in WinGLink, it is important to keep in mind the limitations of the data. First of all is the fact of the skin depth equation, given that the stable signal we recorded ranged from roughly 1Hz to 100Hz, and the modelled resistivity at the near surface ranges roughly from 50 ohm.m to 150 ohm.m, we have a skin depth range of around 300 to 600m for the highest frequencies and 3 to 6km for the lowest frequencies. While this may seem like depths far deeper than the area of interest, it is important to remember that those are the

maximum depths reached by those frequencies, and they contain resistivity/conductance information from the full volume of rock above.

The next important thing to consider is the underlying structure and lithology of the survey area. This survey was situated directly over the top of an east plunging syncline, comprised at the surface of fractured siltstone and limestone, and underlain by various other sediments such as sandstone and shale.

Running east to west along the southern edge of the survey area, across the southern limb of the major syncline is the profile EW1, of which a 2D inversion is shown in figure 4. As is expected, the model's predominant feature is an increasing resistivity with depth. This is consistent with the theory that an increase in depth will generally correspond to an increase in resistivity, due to a decrease in water content and porosity due to increasing pressure (Unsworth *et al.* 2007). It can also be observed that there is a plunge of structure towards the east, consistent with the observed plunge of the axis of the local syncline.

Profile EW2 was positioned to be anchored to the same western edge as EW1, but run in a northeast-southwest direction through the centre of the survey area and along the northern limb of the syncline, a 2D inversion of this profile is shown in figure 5. It shows many of the same features as the profile EW1, including a steady increase in resistivity of from around 30 ohm.m near the surface in places to around 200 ohm.m at depths of around 300m, transitioning up to resistivities of over 300 ohm.m deeper down. This profile also shows the same structural plunge towards the east as seen in EW1. Both profiles show less resistive zones at the surface separated by a zone of more resistive material.

The final east-west oriented profile, EW3 is oriented parallel and to the north of EW1, running through the centre of the survey area, and through the centre of the syncline and along the axial plane. A 2D inversion of this profile is shown in figure 6. It is very similar to the previous EW profiles, showing the same increase in resistivity with depth, from roughly 30 ohm.m near the surface to over 300 ohm.m at 800m. The same structural plunge towards the east is observed, as well as the presence of two less resistive zones at the surface separated by a band of resistive material.

Running roughly north-south, perpendicular to the axis of the syncline, and profiles EW1 and EW3, is the profile NS1, of which a 2D inversion is shown in figure 7. The overall structure of the profile is what would be expected of north-south shortened sediments, with what appears to be multiple folds. The feature highlighted in yellow is where the profile intersects the syncline, with the hinge of the syncline clearly displaying a higher conductivity than the surrounding rock. This could be due to increased water content in the fracture matrix, especially near the hinge, as this would be the area of highest prospectivity for water due to strong axial plane cleavage and maximum potential water column.

The profile NS2 runs roughly parallel to NS1, covering the eastern side of the profile area, a 2D inversion of this profile is shown in figure 8. This profile shows an overall folded structure, with an apparently wider syncline feature than NS1, due to the fact that it intersects the syncline further down the plunge and should therefore appear wider. It also shows an increase in resistivity with an increase in depth, however, the resistivity at depths of around 800m is less than the other profiles, around 200 ohm.m.

Controlled source magnetotelluric data obtained by Zonge engineering in April 2007 were reprocessed and inverted using WinGLink to create a series of 6 profiles in the north-western zone of the survey area. A compilation of these surveys, aligned to show continuation of trends between profiles is shown in figure 9. The main feature is shown by the left arrow; there is a major zone of conductivity on the western edge of each profile, which for profiles 4600, 4900, 5180 and 5450 corresponds to the local creek, which is the recharge zone for the local aquifer. Geologically these zones of higher conductivity correspond to the Mt McKinlay member. The right arrow corresponds to an apparently continuous zone of conductivity.

A pseudo 3D compilation of the 2D inversions was created to show how they relate to each other, as seen in figure 10. This image shows that the different profiles are in agreement with most of the major zones of conductivity and rate of change in resistivity with depth. The intersection of EW1 and NS1 shows a good cross section through the syncline, with EW1 showing the plunge of the hinge and NS1 cutting through and showing the cross section. It can be seen, however, that where NS1 intersects EW2, the two models have very different measures of conductivity for the same area (150 ohm.m compared to about 50 ohm.m). This could be due to differences in profile alignment and fracture alignment. Due to the fact that the profiles have been inverted using TM mode only, which models the electrical conductivity in line with the profile, as opposed to mixed TE/TM mode which also takes into account electrical conductivity running perpendicular to the profile.

The phase tensor ellipses are a way of showing the dimensionality and dominant direction of conductivity at various frequency slices through the survey area, while remaining free of galvanic distortion. Based on Archie's law we can assume that the dominant direction of conductivity is controlled by the alignment of fractures containing saline groundwater. In these plots the elongated axes of the ellipses represent the direction of dominant electrical conductivity, and the fill colour ranging from green to brown represents the level of skew, a measure of the three dimensionality of the phase tensor at that location. A decrease in frequency of the plots will result in an increase in depth sensitivity, while still maintaining information from the overlying volume.

Figure 11 shows a series of phase tensor maps corresponding to 94Hz, 70Hz and 23Hz. 94Hz is the highest non-noisy frequency available in the data, and therefore corresponds to the shallowest skin depth, which, given an average resistivity of around 200 ohm.m is roughly 700 metres. It is important to note however, that these figures still contain conductivity information from the overlying volume, and that if the overlying volume is much more conductive, as it is in this area, it will have a much greater weight on the data. The phase tensors in figure 11 show that for these frequencies the predominant direction of conductivity ranges from north-south to northeast-southwest with some sites showing east-west preference. The 70Hz phase tensors show very similar trends, mostly northeast-southwest; however there are a few northwest-southeast trending tensors, indicating a moderate degree of heterogeneity in direction of electrical conductivity direction. The 23Hz phase tensors correspond to a much deeper level of sensitivity, roughly 1500m. These tensors show a much greater degree of homogeneity, almost entirely aligned northeast- southwest, consistent with the regional structure and syncline. Taken together, these tensor plots show that the regional direction of current flow is consistent with the regional direction of shortening, then as we go to shallower depths, the level of three dimensionality and heterogeneity of electrical conductance increases, ranging from north-south to northeast-southwest. In terms of hydrogeology, the phase tensors are most consistently aligned northeast-southwest near the axis of the syncline

and along Mt McKinlay creek, this can be interpreted that these areas provide the most consistent signal because they are the most conductive in the area, due to the fractures in these zones being saturated. Areas with unsaturated fractures would have a poorer contrast in conductivity between the fractures and matrix, and would therefore be more subject to more subtle changes in the rock volume aside from fractures. Therefore these zones may contain more water in their fractures.

A pseudo-section of profile NS1 is shown in figure 12. Pseudo-sections display the phase and apparent resistivity in terms of frequency across the profile before modelling, and are a good way to check for any obvious noise and inconsistencies in the data. This section is typical of the other pseudo-sections, showing changes in phase and resistivity with frequency. Worth noting is the zone of higher apparent conductivity highlighted by the yellow arrow corresponding to the location of the profile intersection the axis of the syncline.

Current water production from bores for the Nipapanha community is from bores 149 and 101, with rates of 12L/s and 2.2L/s respectively. Bore 149 is located at the midway point along Zonge profile 5450, in between the northern ends of the NS profiles. This does correspond to a zone of higher conductivity on the 5450 profile, which seems to be continuous along the other profiles as well. Bore 101 is located just to the east of profile EW3, which is located along the hinge of the syncline. The eastern edge of this profile shows a comparatively higher degree of conductivity (around 50 ohm.m), which could correspond to a higher concentration of water filled fractures, as bore 101 indicates there is at least some water in the area.

Conclusion

As a proof of concept, the aim of this survey was to compare results and conclusions from previous geophysical, structural and hydrogeological surveys in order to gain an insight into the strengths and weaknesses of using magnetotellurics to characterize fractured rock aquifers in other areas, without previous work to rely on. It is important to note that due to the relatively poor resolution of magnetotelluric data at shallow depths, these surveys should not be used as the sole tool for planning a drilling program, rather, they should be used as part of a more comprehensive investigation, and will only give outputs to reduce the risk of drilling dry boreholes as opposed to be guaranteeing drilling a productive one.

When comparing the survey results to previous work, there is a level of confidence where one could make recommendations to reduce the risk of drilling dry boreholes based on MT surveys. In terms of comparing the survey with hydrogeological data, the currently producing boreholes in the area, 149 and 101 as well as their geological unit correspond to apparent zones of higher apparent conductivity than surrounding rock. The structural investigations of the area identified an east-west trending syncline that plunges towards the east, which is confirmed by the combination of the east-west and north-south profiles showing both the plunge of the syncline and resolving the extent of the axis and limbs in the area surveyed. There is very little overlap between the Zonge survey and the magnetotelluric survey carried out for this project, but where they do there is reasonable level of similarity between apparent resistivity values.

In conclusion, a combination of magnetotelluric inversion and phase tensor analysis combined with structural and hydrogeological knowledge has identified a potential zone of higher bulk porosity in the axis of the syncline. Magnetotelluric investigations show zones of higher apparent conductivity,

structural analysis identifying it as a zone of strong axial plane cleavage, and hydrogeological analysis targeting the Wilkawillina Limestone in the syncline axis for its favourable aquifer properties.

References

ARANGO C., MARCUELLO A., LEDO J. & QUERALT P. 2009. 3D magnetotelluric characterization of the geothermal anomaly in the Llucmajor aquifer system (Majorca, Spain). *Journal of Applied Geophysics* **68**, 479-488.

BIBBY H. M., CALDWELL T. G. & BROWN C. 2005. Determinable and non-determinable parameters of galvanic distortion in magnetotellurics. *Geophysical Journal International* **163**, 915-930.

CALDWELL T. G., BIBBY H. M. & BROWN C. 2004. The magnetotelluric phase tensor. *Geophysics Journal International* **158**, 457-469.

CHANDRASEKHAR E., FONTES S. L., FLEXOR J. M., RAJARAM M. & ANAND S. P. 2009. Magnetotelluric and aeromagnetic investigations for assessment of groundwater resources in Parnaiba basin in Piaui State of North-East Brazil. *Journal of Applied Geophysics* **68**, 269-281.

CHAVE A. D. & THOMSON D. J. 2003. A bounded influence regression estimator based on the statistics of the hat matrix. *Journal of the Royal Statistical Society: Series C (Applied Statistics)* **52**, 307-322.

COOK P. G. 2003. *A guide to regional groundwater flow in fractured rock aquifers*. CSIRO Australia.

COSTAR A., DODDS S. & SAMPSON L. 2008. Nepabunna Community Hydrogeological and Geophysical Investigation Report. *Knowledge and Information Division Department of Water, Land and Biodiversity Conservation* **DWLBC Report 2008/24**.

COSTAR A., HOWLES S. & KRUGER N. 2009. Aboriginal lands town water supply – Nepabunna, Far North, South Australia. *Science, Monitoring and Information Division Department of Water, Land and Biodiversity Conservation* **DWLBC Report 2009/XX**.

DYSON I. A. 1998. Neoproterozoic salt tectonics and sequence boundary formation in the Adelaide Geosyncline. *Geological Society of Australia Abstracts* **51**, 44-45.

DYSON I. A. 1999. The Beltana Diapir: a salt withdrawal mini-basin in the northern Flinders Ranges. *Mines and Energy of South Australia Journal* **15**, 40-46.

DYSON I. A. 2005. Evolution of allocthonous salt systems during development of a divergent margin: the Adelaide Geosyncline of South Australia GCSSEPM 25th Bob F. Perkins Research Conference, Houston, Texas (unpubl.).

FAYBISHENKO B. 2000. Dynamics of fluids in fractured rock. *Geophysical Monograph Series* **122**, ix-x.

GARCIA X., LEDO J. & QUERALT P. 1999. 2D inversion of 3D magnetotelluric data: The Kayabe dataset. *Earth Planets Space* **51**, 1135-1143.

MOECK I., DUSSEL M., TROGER U. & SCHANDELMEIER H. 2007. Fracture networks in Jurassic carbonate rock of the Algarve Basin (South Portugal): Implications for aquifer behaviour related to the recent stress field. *In:* Krasny J. & Sharp J. M. eds., *Groundwater in fractured rocks*, Taylor & Francis Group, London.

NEWMAN G. A., HOVERSTEN G. M., WANNAMAKER P. E. & GASPERIKOVA E. 2008. 3D Magnetotelluric characterization of the Coso Geothermal Field. *Lawrence Berkeley National Laboratory, Earth Sciences Division*.

PAUL E., FLÖTTMANN T. & SANDIFORD M. 1999. Structural geometry and controls on basement-involved deformation in the northern Flinders Ranges, Adelaide Fold Belt, South Australia. *Australian Journal of Earth Sciences* **46**, 343-354.

RAYNER S., BENTLEY L. & ALLEN D. 2007. Constraining Aquifer Architecture with Electrical Resistivity Imaging in a Fractured Hydrogeological Setting. *Journal of Environmental and Engineering Geophysics* **12**, 323-335.

READ R. E. 1981. Nepabunna water supply, 1980 drilling programme. *Department of Mines & Energy South Australia* **Report Book 81/13**.

SIMPSON F. & BAHR K. 2005. *Pratical Geophysics* (Vol. 1). Cambridge University Press, Cambridge.
SKINNER D. & HEINSON G. 2004. A comparison of electrical and electromagnetic methods for the detection of hydraulic pathways in a fractured rock aquifer, Clare Valley, South Australia. *Hydrogeology Journal* **12**, 576-590.
SMIRNOV M., KORJA T., DYENSIUS L., PEDERSEN L. B. & LAUKKANEN E. 2008. Broadband Magnetotelluric Instruments for Near-surface and Lithospheric Studies of Electrical Conductivity: A Fennoscandian Pool of Magnetotelluric Instruments. *Geophysica* **44(1-2)**, 31-44.
TURBERG P., MULLER I. & FLURY F. 1994. Hydrogeological investigation of porous environments by radio magnetotelluric-resistivity (RMT-R 12-240 kHz). *Journal of Applied Geophysics* **31**, 133-145.
UNSWORTH M., SOYER W., TUNCER V., WAGNER A. & BARNES D. 2007. Hydrogeologic assessment of the Amchitka Island nuclear test site (Alaska) with magnetotellurics. *Geophysics* **72**, B47-B57.

Figures

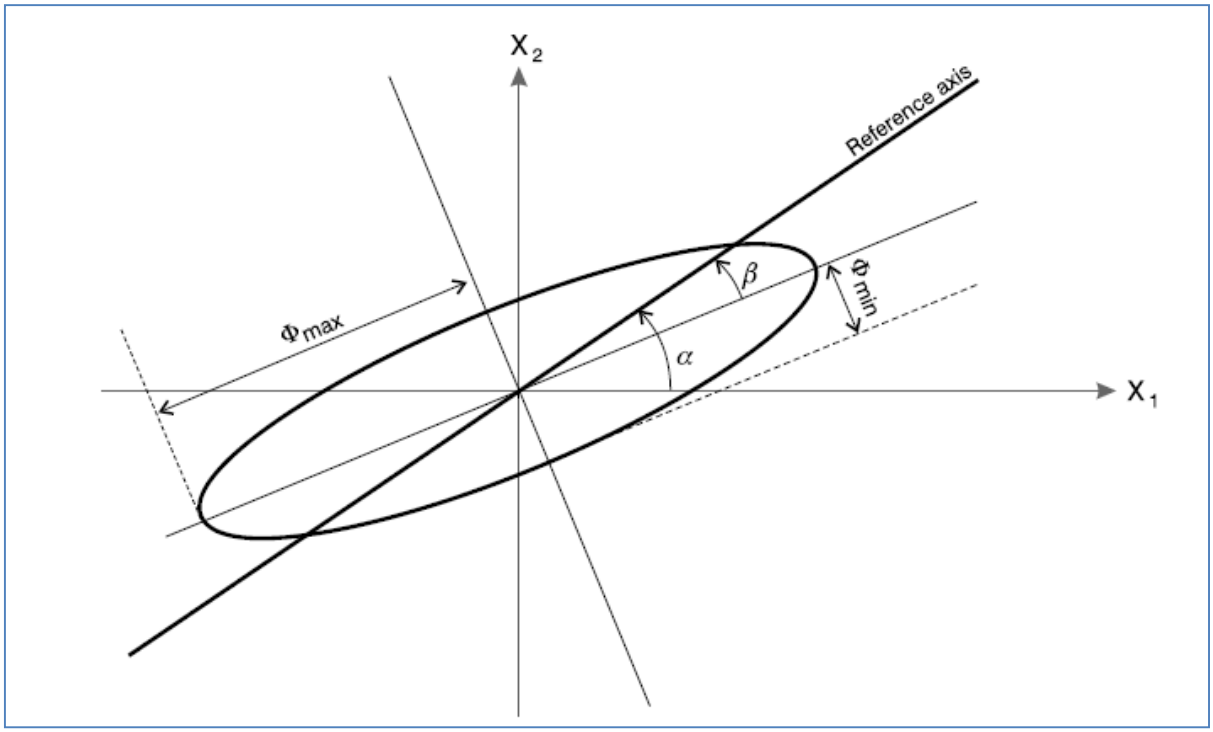

Figure 1 - Diagram of phase tensor ellipse showing how Φmax, Φmin, α and β affect the shape and orientation of the ellipse. Figure from (Bibby *et al.* 2005).

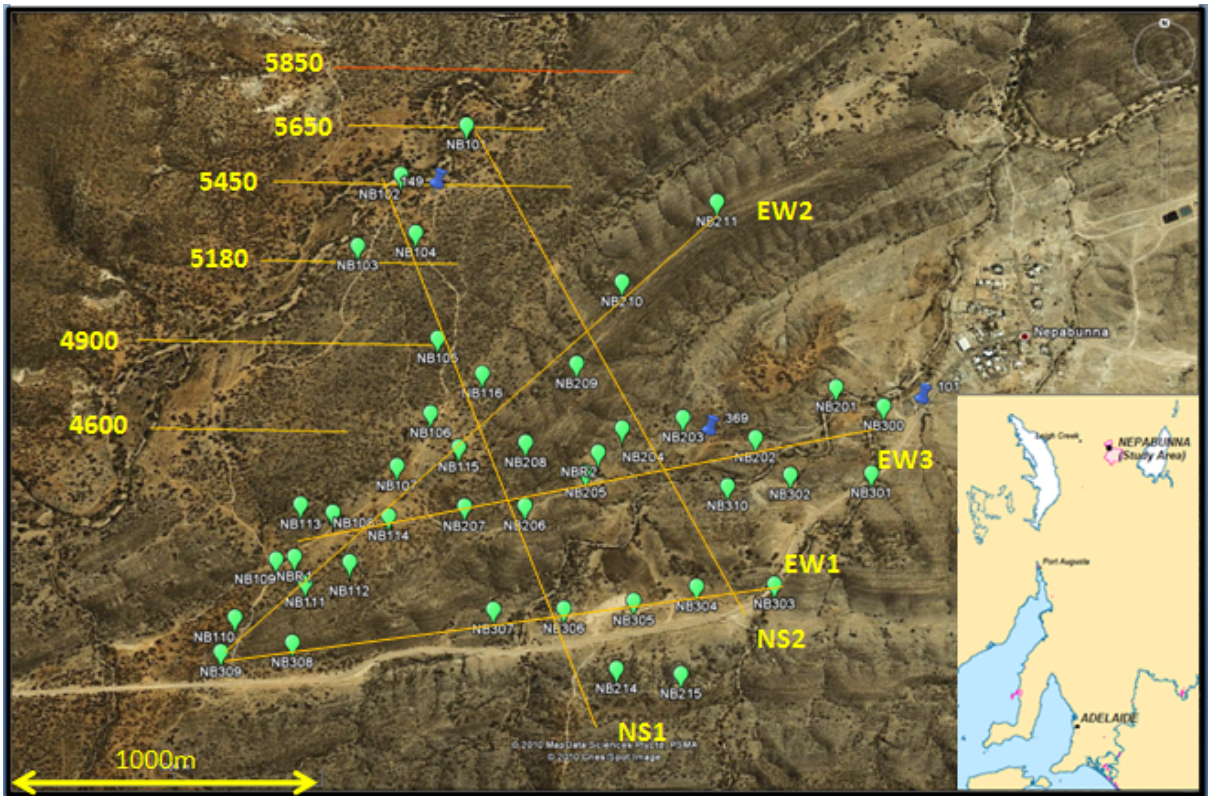

Figure 2 Satellite image of the study area with profiles shown as yellow lines and producing bores shown as blue pins, with inset of location

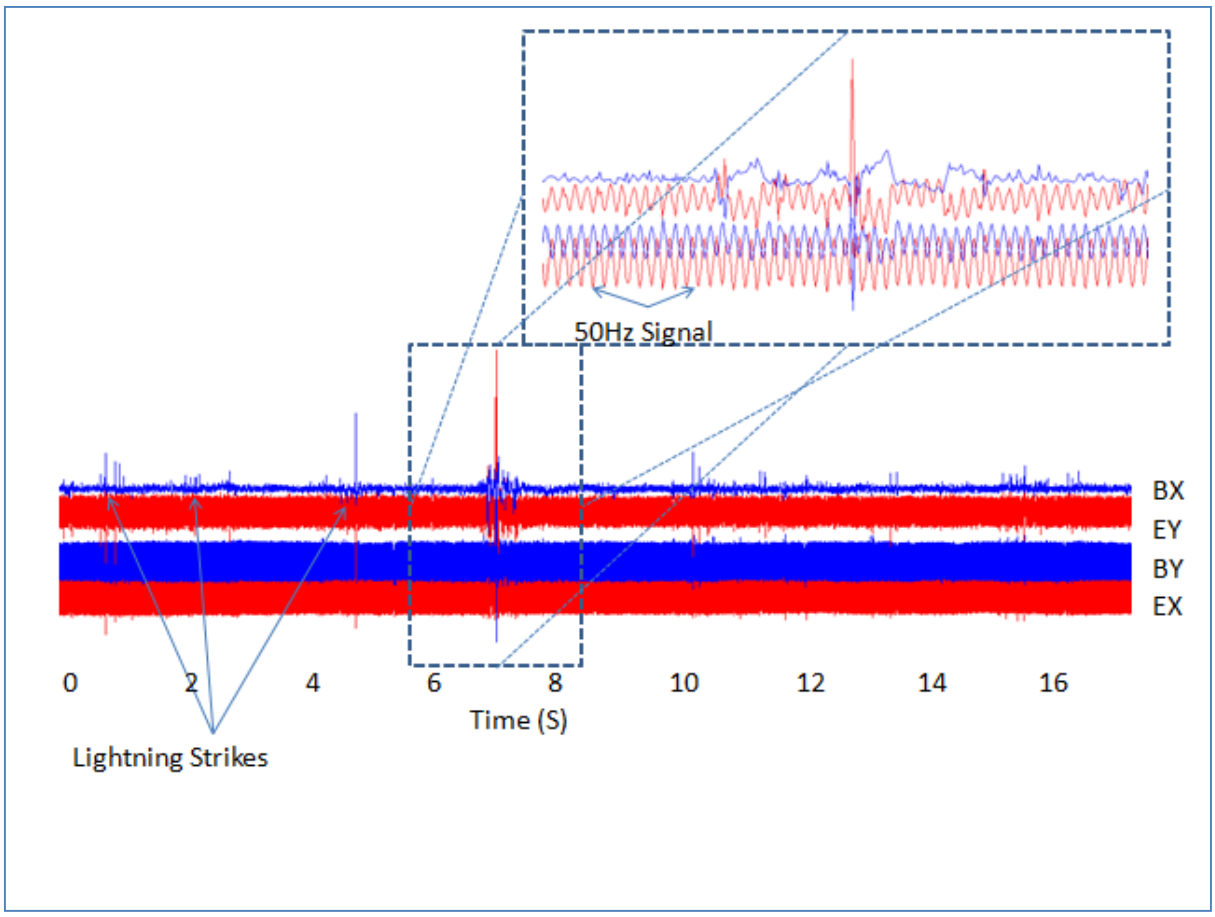

Figure 3 - Time series plot of typical 4 channel MT data showing lightning strike responses and 50Hz noise

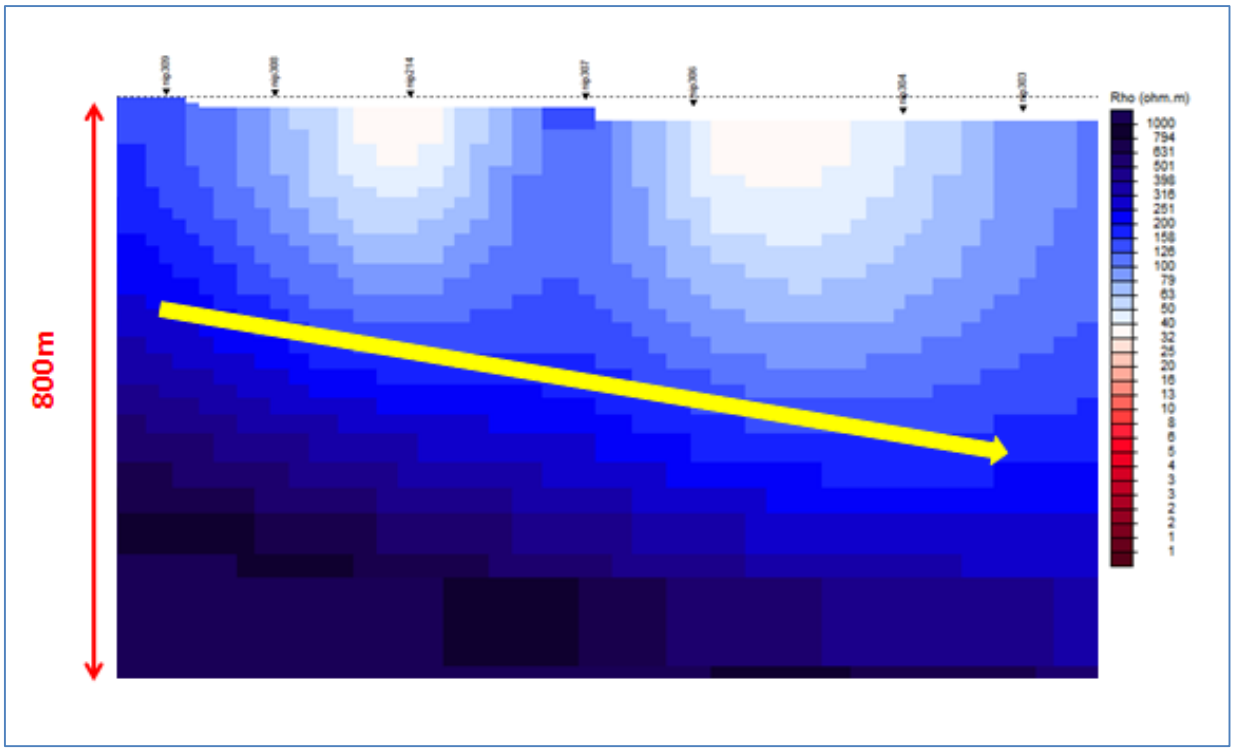

Figure 4 – Profile EW1, major features are increasing apparent resistivity with depth, plunge of structure towards the east and two zones of higher apparent conductivity separated by a resistive band. RMS error of 3.8.

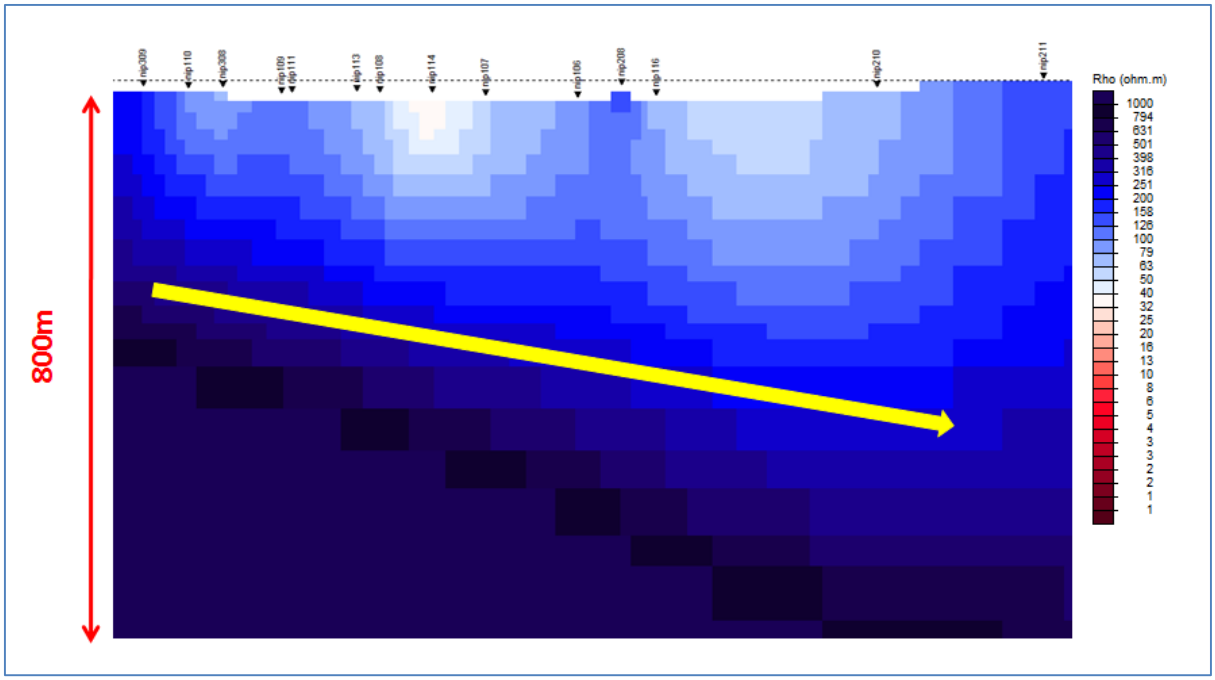

Figure 5 – Profile EW2, major features are structural plunge towards the east, three higher conductivity zones near the surface separated by resistive bands, an increase in apparent resistivity with depth. RMS error of 5.9.

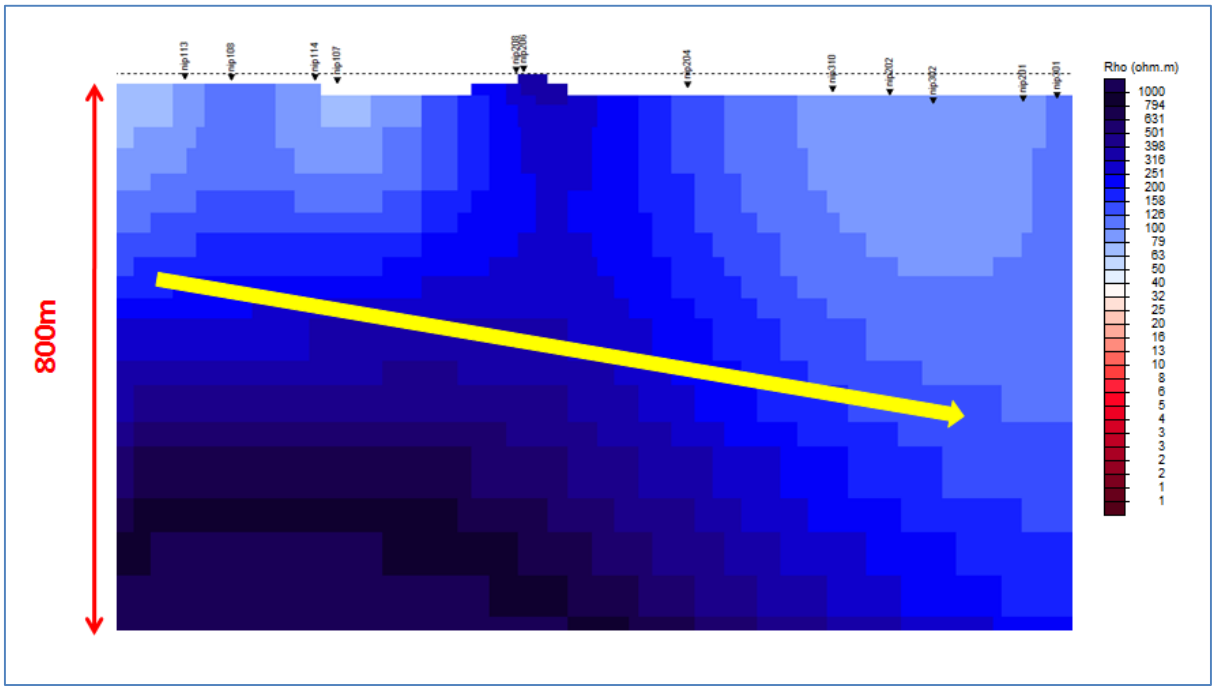

Figure 6 – Profile EW3, major features are a structural plunge towards the east, higher conductivity eastern and western ends of the profile separated by a resistive band and an increase in apparent resistivity with depth. RMS error of 6.8.

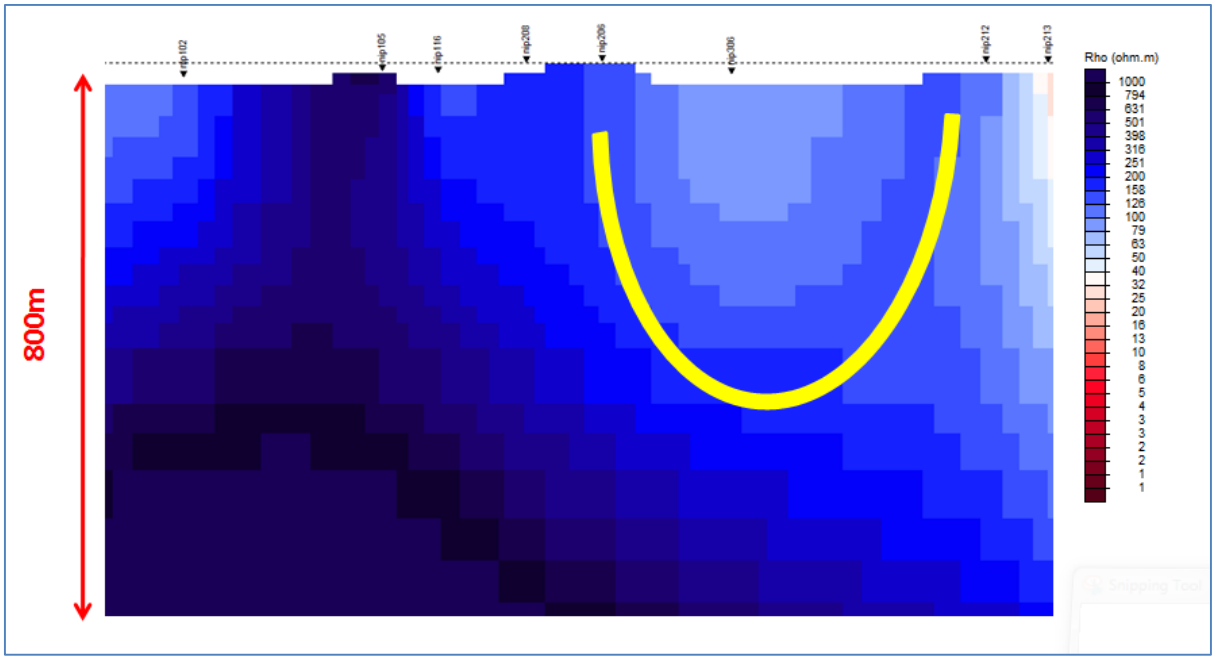

Figure 7 – Profile NS1, feature highlighted in yellow is interpreted as the major syncline in the Nepabunna area, with the axis of the syncline corresponding to the area of highest apparent conductivity. RMS error of 4.6.

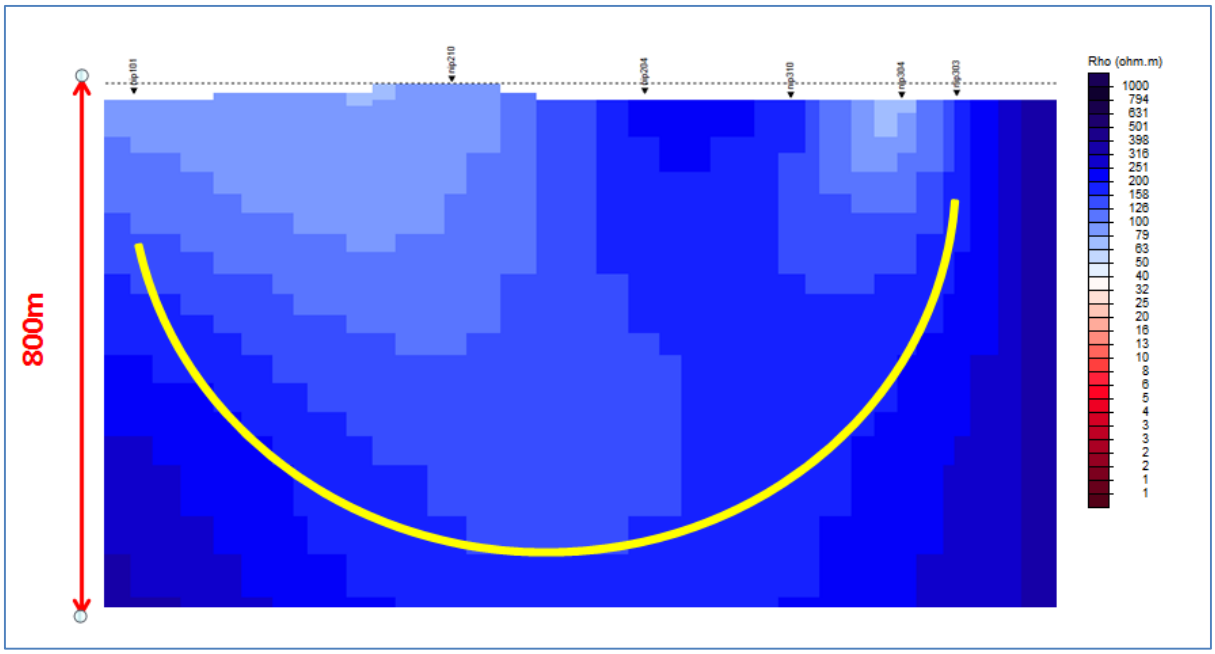

Figure 8 – Profile NS2, feature highlighted in yellow interpreted to show major syncline, with two areas of higher apparent conductivity. RMS error of 6.8.

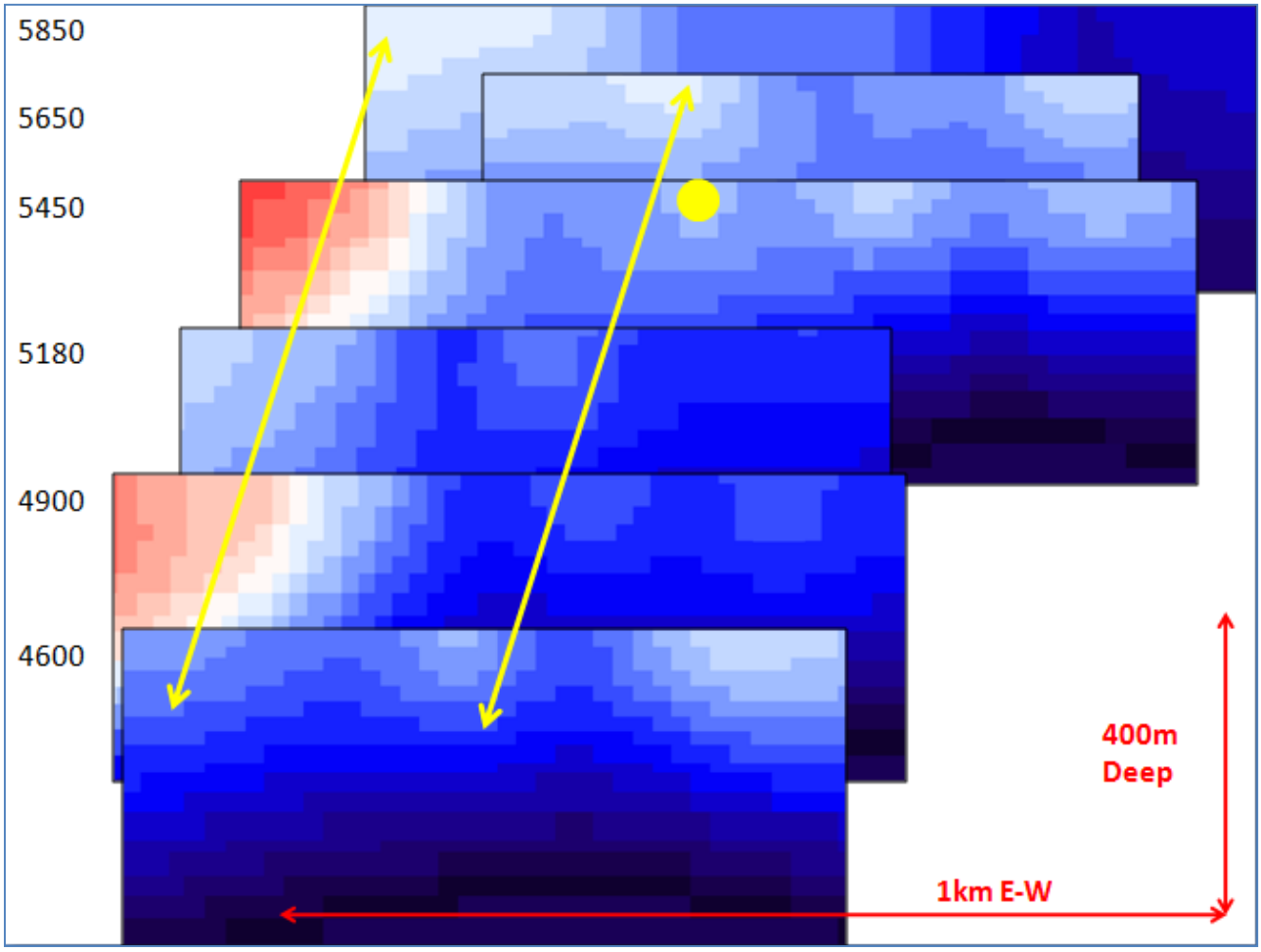

Figure 9 – Compilation of Zonge CSAMT profiles with the southmost profile at the bottom of the image. Features indicated by yellow arrow are zones of continuous resistivity anomalies. Yellow Dot represents production bore 149.

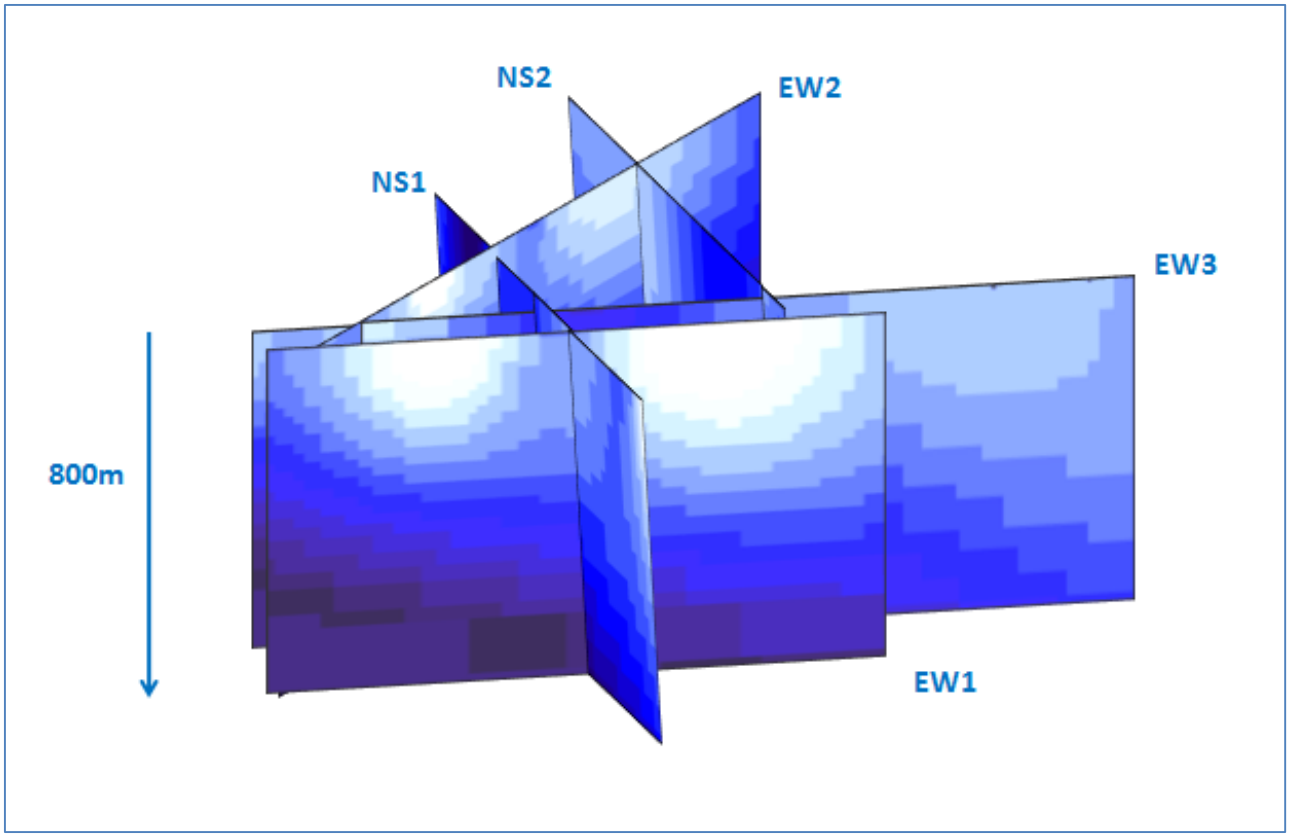

Figure 10 – Pseudo 3D image of profiles, demonstrating overall structure of the survey area, a syncline plunging to the east with various zones of higher apparent conductivity.

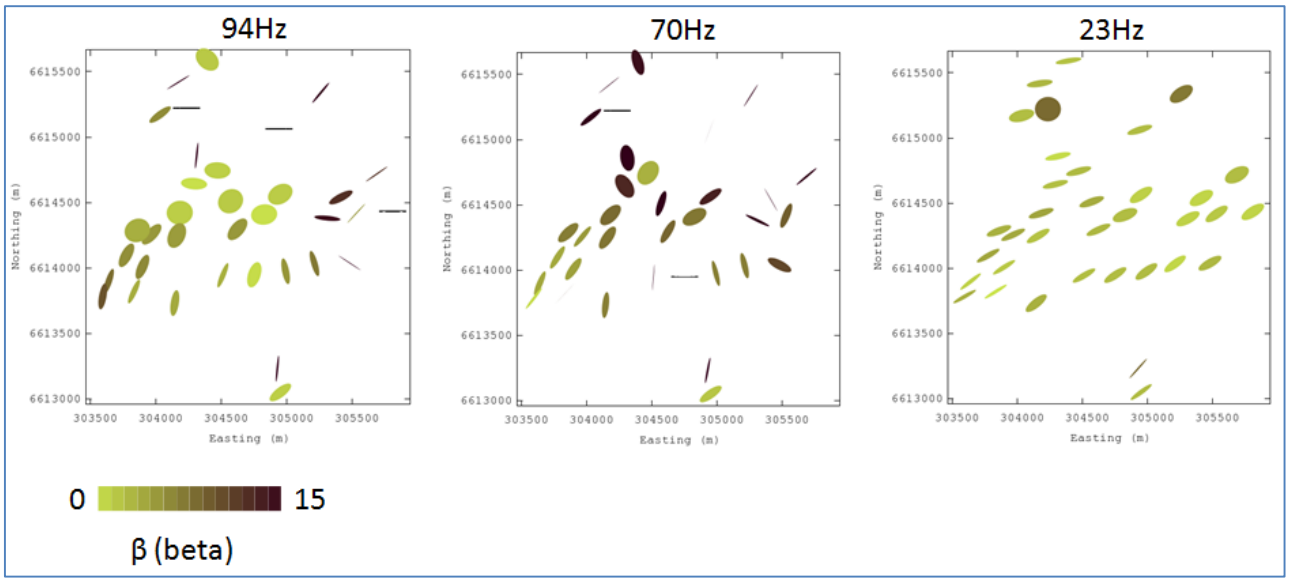

Figure 11 – Phase tensors covering 94hz, 70Hz and 23Hz. The colour scale from green to brown indicates the level of skew or three dimensionality present for that tensor. Tensors appearing as flat lines are sites of excessive noise for those frequencies and cannot be displayed.

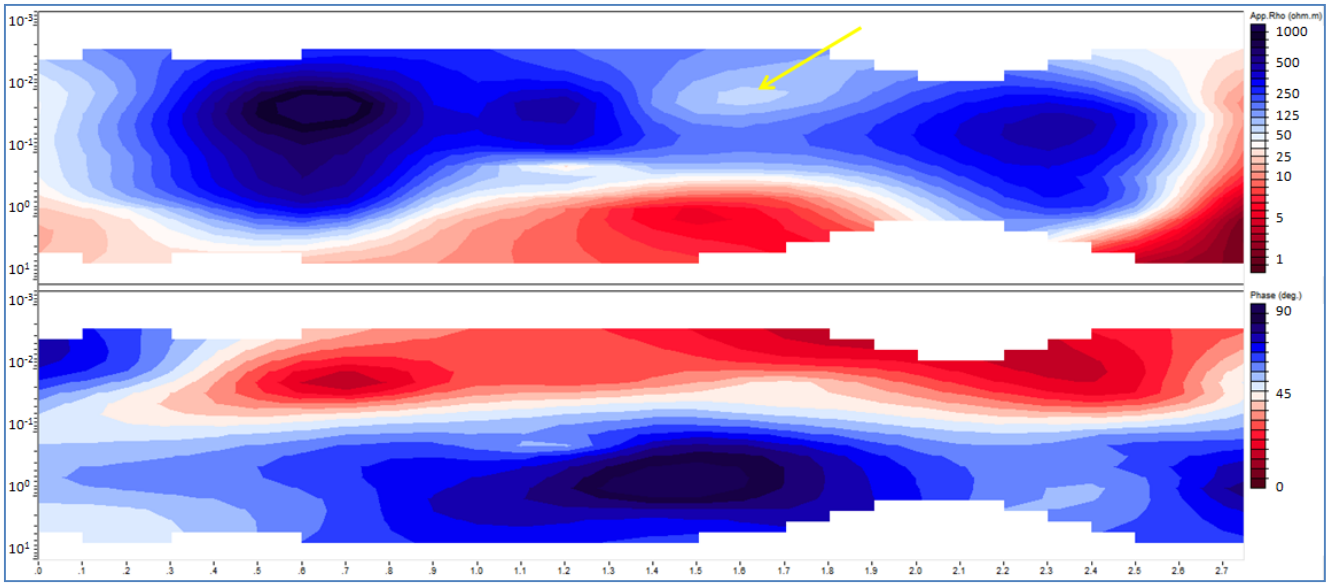

Figure 12 - Pseudo section of profile NS1 showing apparent resistivity and phase vs frequency. The yellow arrow is pointing to intersection with the axis of the syncline.